Thermal Proteome Profiling Reveals Glutathione Peroxidase 4 as the Target of the Autophagy Inducer Conophylline[S]

Junya Kakegawa, Satoshi Ohtsuka, Masahiro Yokoyama, Toru Hosoi, Koichiro Ozawa, and Takashi Hatanaka

Pharmaceutical Frontier Research Laboratories, Central Pharmaceutical Research Institute, Japan Tobacco Inc., Kanagawa, Japan (J.K., S.O., M.Y., T.Ha.); Department of Clinical Pharmacology, Faculty of Pharmaceutical Sciences, Sanyo-Onoda City University, Yamaguchi, Japan (T.Ho.); and Department of Pharmacotherapy, Graduate School of Biomedical and Health Sciences, Hiroshima University, Hiroshima, Japan (K.O.)

ABSTRACT

Conophylline (CNP) is a vinca alkaloid extracted from the *Tabernaemontana divaricata* plant. It has been reported that CNP induces autophagy in a mammalian target of rapamycin–independent manner, and thereby inhibits protein aggregation. However, the mode of action of CNP in inducing autophagy remains unknown. In this study, we identified glutathione peroxidase 4 (GPX4) as a CNP-binding protein by using thermal proteome profiling. The technique exploits changes in the thermal stability of proteins resulting from ligand interaction, which is capable of identifying compound-binding proteins without chemical modification. GPX4, an antioxidant protein that uses reduced glutathione as a cofactor, directly catalyzes the reduction of hydrogen peroxide, organic hydroperoxides, and lipid peroxides. GPX4 suppresses lipid peroxide accumulation, and thus plays a key role in protecting cells from oxidative damage. We found that treatment with CNP caused accumulation of lipid reactive oxygen species (ROS) in cultured cells. Furthermore, similarly with CNP treatment, GPX4 deficiency caused accumulation of lipid ROS and induced autophagy. These findings indicate that GPX4 is a direct target of CNP involved in autophagy induction.

SIGNIFICANCE STATEMENT

The present study identified glutathione peroxidase 4 (GPX4) as a binding protein of conophylline (CNP) by using thermal proteome profiling (TPP). This study showed that CNP treatment, similarly with the inhibition of GPX4, induced lipid reactive oxygen species accumulation and autophagy. The present findings suggest that GPX4 is the CNP target protein involved in autophagy induction. Furthermore, these results indicate that TPP is a useful technique for determining the mechanism of natural compounds.

Introduction

Natural compounds possess unique structures and occupy more diverse chemical spaces compared with the majority of synthetic small molecules (Feher and Schmidt, 2003; Rosén et al., 2009). They have various physiologic activities, and are expected to be particularly useful as lead compounds for drug development (Lachance et al., 2012). Indeed, it has been reported that 34% of the medicines approved by the US Food and Drug Administration between 1981 and 2010 are natural compound derivatives (Harvey et al., 2015; Newman and Cragg, 2016). The compounds are usually obtained from cell-based screening, so that in many cases, the exact target proteins and precise mode of action of the compounds are unknown. The elucidation of the mechanisms of the compounds has attracted attention because of the expectation that the investigation will uncover novel biologic mechanisms. Here, we present a mechanism of a natural compound with various in vitro and in vivo effects.

Conophylline (CNP) is a vinca alkaloid isolated from the ethanolic extract of *Tabernaemontana divaricata* leaves (Kam et al., 1993). It has been reported that CNP treatment may be effective for various diseases. In the first report to investigate the CNP effects on cells, CNP was shown to induce morphologic normalization of kirsten rat sarcoma viral oncogene homologue–overexpressing cancer cells (Umezawa et al., 1994). In addition, administration of CNP has also been shown to improve disease conditions in various animal models, including diabetes (Umezawa et al., 2003; Ogata et al., 2004), nonalcoholic steatohepatitis (Ohashi et al.,

ABBREVIATIONS: ARL6ip1, ADP-ribosylation factor–like protein 6–interacting protein 1; ATG, autophagy-related protein; Baf.A1, bafilomycin A1; CCR, compound concentration range; CNP, conophylline; GAPDH, glyceraldehyde 3-phosphate dehydrogenase; GPX4, glutathione peroxidase 4; HEK, human embryonic kidney; JNK, c-Jun N-terminal kinase; LC3, microtubule-associated protein 1 light chain 3; LC-MS/MS, liquid chromatography-tandem mass spectrometry; MS, mass spectrometry; mTOR, mammalian target of rapamycin; p70S6K, p70 S6 kinase; RFP, red fluorescent protein TagRFP; ROS, reactive oxygen species; RPS6, S6 ribosomal protein; siRNA, small interference RNA; Tm, melting temperature; TMT, tandem mass tag; TPP, thermal proteome profiling; TR, temperature range.

2019), and lung fibrosis (Saito et al., 2012; Tezuka et al., 2018). Furthermore, it has been reported that CNP suppresses aggregation of mutant huntingtin in cells by inducing autophagy (Sasazawa et al., 2015). Therefore, various effects of CNP treatment may be related to the activity of inducing autophagy.

Autophagy is a cellular mechanism for bulk degradation of cytosolic components, including organelles. Autophagy is initiated by the sequestration of cytoplasmic components in double-membrane structures, called autophagosomes, and is mediated by evolutionarily conserved autophagy-related genes (ATGs) and microtubule-associated protein 1 light chain 3 (LC3). The autophagosome fuses with a lysosome to form an autolysosome, and then the autophagosome-delivered contents and its inner membrane are degraded by lysosomal hydrolase (Ohsumi, 2001; Galluzzi et al., 2017). Autophagy plays crucial roles in protein homeostasis and maintenance of cellular function and viability by eliminating aggregated protein or dysfunctional organelles. In recent years, its role in the prevention of cancer, neurodegenerative diseases, diabetes, nonalcoholic steatohepatitis, and fibrotic diseases has been recognized (Mizushima, 2018; Mizushima and Levine, 2020). Indeed, autophagy suppressor rubicon-knockout mice reduced α-synuclein accumulation in the brain or interstitial fibrosis in kidney (Nakamura et al., 2019). In addition, nilotinib, which is an oral breakpoint cluster region-abelson tyrosine kinase inhibitor, induces autophagy and promotes α-synuclein clearance (Mahul-Mellier et al., 2014). Thus, elucidation of the mechanism of CNP-induced autophagy can explain CNP's attractive effects in vivo, which may lead to new therapeutic approaches for various diseases.

In the present study, we used thermal proteome profiling (TPP) to investigate the mode of action of CNP in the induction of autophagy. The TPP technique was used based on the principle that the thermal stability of proteins will change upon interaction with ligands, such as small molecules or natural compounds (Savitski et al., 2014). Interestingly, we identified phospholipid hydroperoxide glutathione peroxidase 4 (GPX4) as a CNP-binding protein using this technique. GPX4 is an antioxidant protein that suppresses lipid oxidation in cells. Based on this finding, we examined the effects of CNP on lipid oxidation. In addition, we explored whether GPX4 inhibition leads to induction of autophagy. From this study, we propose that TPP is a useful technique for target identification of natural compounds, and for elucidating the molecular mechanisms of CNP-induced autophagy.

Materials and Methods

Cell Lines, Antibodies, Compounds, Reagents. The U-2 OS (human osteosarcoma) cell line and HEK293T (human embryonic kidney) cell line were obtained from the American Type Culture Collection (Manassas, VA). U-2 OS cells were maintained in McCoy's 5a modified medium supplemented with 10% (v/v) fetal bovine serum and 1% (v/v) penicillin-streptomycin solution (Sigma-Aldrich, St. Louis, MO) in a humidified CO_2 incubator. HEK293T cells were maintained in Dulbecco's modified Eagle's medium supplemented with 10% (v/v) fetal bovine serum and 1% (v/v) penicillin-streptomycin solution (Sigma-Aldrich). The primary antibodies were as follows: anti-α-tubulin (T5168) from Sigma-Aldrich; anti-GPX4 (sc-166120) from Santa Cruz Biotechnology (Dallas, TX); anti-LC3B (186-3) and ATG7 (PM039) from MBL (Nagoya, Japan); anti-phospho-p70 S6 kinase (Thr389) (9234), p70 S6 kinase (2708), phospho-S6 ribosomal

protein (4858), and S6 ribosomal protein (2217) from Cell Signaling Technology, Inc. (Danvers, MA). Secondary antibodies conjugated horseradish peroxidase were purchased from Agilent Technologies, Inc. (Santa Clara, CA). The compounds CNP (BioBioPha Co., Ltd., Kunming, China), Torin 1 (Tocris Bioscience, Bristol, UK), ML210 (MedChemExpress, Monmouth Junction, NJ), erastin (MedChemExpress), and bafilomycin A1 (Sigma-Aldrich) were dissolved in DMSO (Wako Pure Chemical Industries, Ltd., Osaka, Japan) before being diluted with cell culture medium. Boron-dipyrromethene 581/591 C11 were obtained from Thermo Fisher Scientific, Inc. (Waltham, MA).

Generation of the RFP-GFP-LC3 Stably Expressed Cell Line. The cDNAs of red fluorescent protein TagRFP (RFP) (Evrogen, Moscow, Russia), green fluorescent protein TagGFP2 (Evrogen), and LC3B (Promega, Madison, WI) were cloned into a pLVSIN-EF1α-Pur vector (Takara Bio Inc., Shiga, Japan). HEK293T cells were transfected with the plasmid and lentiviral high titer packaging mix using LipofectAMINE 3000 transfection reagent (Thermo Fisher Scientific). Two days later, the supernatants were used for transduction into U-2 OS cells. GFP-positive cells were sorted by a BD FACSAria Cell Sorter (BD Biosciences, San Jose, CA), and then single-cell clones were isolated by limiting dilution. The cells were maintained in McCoy's 5a modified medium supplemented with 10% (v/v) fetal bovine serum, 1% (v/v) penicillin-streptomycin solution (Sigma-Aldrich), and 0.3 μg/ml puromycin (Thermo Fisher Scientific) in a humidified CO_2 incubator.

Detection of the LC3 Dot Formation. U-2 OS cells were seeded onto 96-well, μClear black microplates (6×10^3 cells/well) (Greiner Bio-One GmbH, Kremsmünster, Austria). On the next day, the cells were treated with compounds for 3 hours at 37°C and were fixed with 4% paraformaldehyde in PBS (Wako Pure Chemical Industries, Ltd.). The cells were incubated with PBS containing 50 mM NH_4Cl for 15 minutes, 50 μg/ml digitonin for 10 minutes, and then 0.2% gelatin for 60 minutes at room temperature. Then, the cells were incubated with anti-LC3 antibody for 60 minutes, anti-rabbit IgG-conjugated Alexa Fluor 488 (Thermo Fisher Scientific) for 30 minutes, and then PBS containing 1 μg/ml Höechst 33258 (Thermo Fisher Scientific) for 15 minutes at room temperature. LC3 puncta were visualized using confocal microscopy (Nikon, Tokyo, Japan). RFP-GFP-LC3 stably expressed U-2 OS cells were seeded onto a 96-well μClear black microplate as described above, treated with compounds, and then fixed with 4% paraformaldehyde in PBS containing Höechst 33258. LC3 puncta were visualized and quantified using Operetta CLS (PerkinElmer, Waltham, MA).

TPP of Proteins in Cell Extracts. The TPP experiments were performed as described in previous reports with some modifications (Savitski et al., 2014). Briefly, U-2 OS cells (1×10^8 cells) in a tube were suspended in ice-cold PBS containing EDTA-free protease inhibitor cocktail (Sigma-Aldrich) and snap-frozen in liquid nitrogen. The tube was placed into a water bath at 23°C until a portion of the content was thawed and then transferred onto ice until the entire content was thawed. This freeze/thaw cycle was repeated two more times, and then the samples were centrifuged at 100,000g for 20 minutes at 4°C. The supernatants were collected, and then the protein concentrations of the supernatants were determined by advanced protein assay reagent (Cytoskeleton, Inc., Denver, CO).

In the TPP-temperature range (TR) experiments, 100 μM conophylline or DMSO alone were added to the cell extracts, respectively, to a final DMSO concentration of 1%, and incubated for 10 minutes at 23°C. Each extract was divided into 10 aliquots and individually heated for 3 minutes at dierent temperatures: 40°C, 43°C, 46°C, 49°C, 52°C, 55°C, 58°C, 61°C, 64°C, and 67°C, followed by 3 minutes at 23°C. Subsequently, the samples were centrifuged at 14,000g for 20 minutes at 4°C, and then the supernatants were used for liquid chromatography-tandem mass spectrometry (LC-MS/MS). In the TPP-compound concentration range (CCR) experiments, the cell extracts were incubated with vehicle or CNP over a range of nine concentrations, then heated at 55°C and subsequently treated in the same manner as described above.
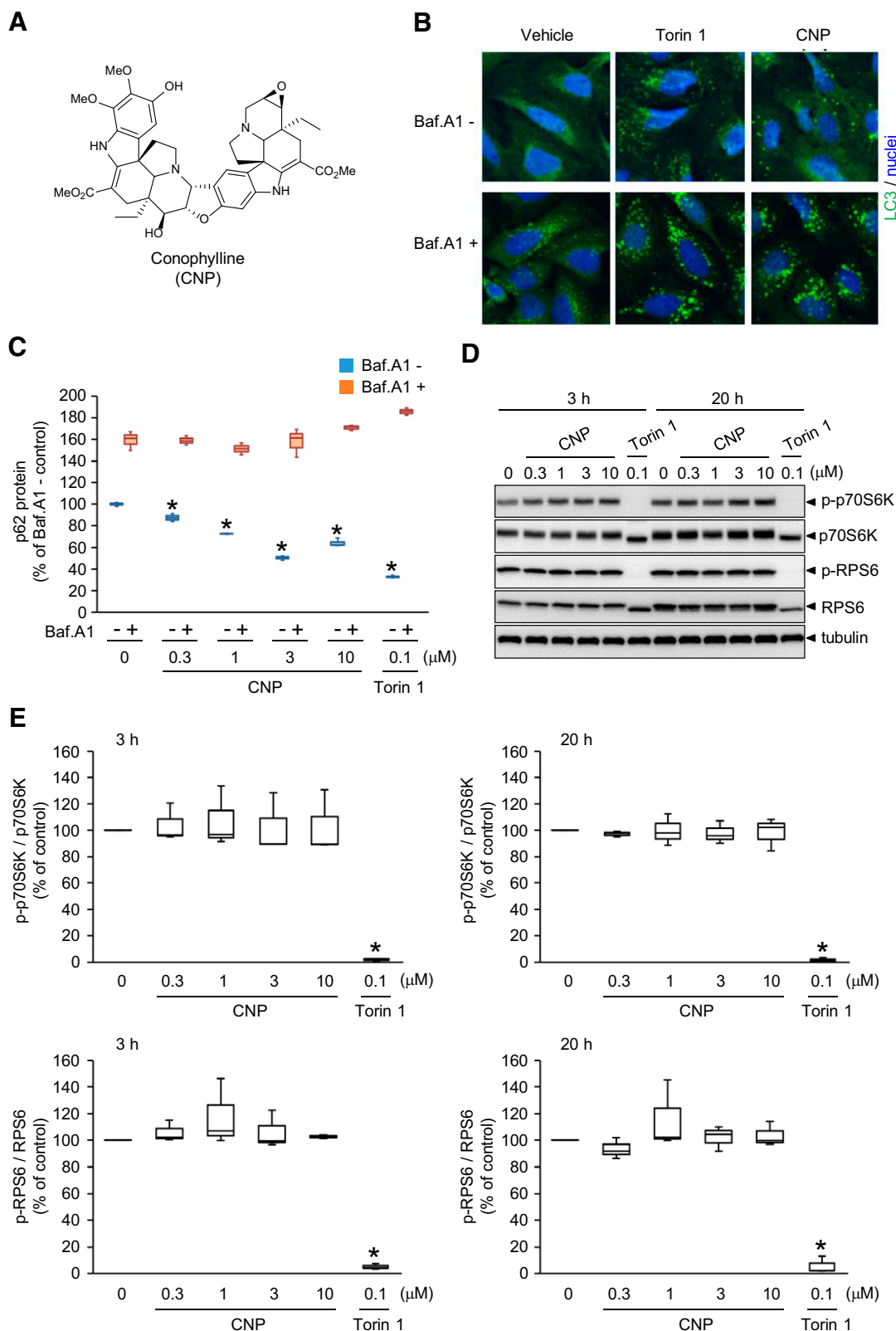
A

Conophylline
(CNP)

B

C

D

E

Fig. 1. Chemical structure of CNP and the autophagy-inducing activity of CNP in U-2 OS cells. (A) The chemical structure of CNP. (B) U-2 OS cells were incubated for 3 hours in the presence of DMSO as vehicle, 0.1 μM Torin 1, or 10 μM CNP with or without 0.1 μM Baf.A1. The cells were fixed with 4% formaldehyde and stained for LC3 (green) and nuclei (blue) described in *Materials and Methods*. The cells were observed by confocal microscopy. (C) U-2 OS cells were incubated for 20 hours in CNP, Torin 1 with or without 0.1 μM Baf.A1 at the indicated concentrations. The cells were lysed, and p62 protein levels were measured by AlphaLISA as described in *Materials and Methods*. The p62 protein levels were normalized to the total protein levels, and expressed as percent of vehicle control. Data are represented by box plots ($n = 3$ biologic replicates). *$P < 0.05$ (one-way ANOVA with Dunnett's test) compared with Baf.A1-untreated vehicle control. (D and E) U-2 OS cells were incubated for 3 or 20 hours in the presence of the indicated compounds. The cells were lysed and analyzed by Western blotting using antibodies specific to the

LC-MS/MS Analysis. Samples from each condition were digested with trypsin overnight at 37°C and then precipitated using a methanol-chloroform precipitation method. After protein recovery, samples were reduced with dithiothreitol and alkylated with iodoacetamide. The peptides were labeled with tandem mass tag (TMT) 10-plex reagent (Thermo Fisher Scientific). The 10 labeled samples were mixed and separated into 16 fractions for TPP-TR or 9 fractions for TPP-CCR using reversed phase chromatography at a pH of 12, and then analyzed by Ultimate 3000 nano-liquid chromatography coupled with Q Exactive Plus mass spectrometer (Thermo Fisher Scientific).

Protein Identification and Quantification. The raw files obtained from LC-MS/MS analysis were processed by Proteome Discoverer version 2.0 (Thermo Scientific, Inc.). The identification of proteins was performed against the UniProt human protein database using the built-in SEQUEST HT, MS Amanda and connected Mascot engine. The parameters were set to 10 ppm mass tolerance for peptide precursors and 0.02 Da tolerance for fragment ions. Trypsin was used as the digesting enzyme, and three missed cleavages were allowed. The TMT modification of lysine residues were set as fixed modifications, whereas methionine oxidation, N-terminal acetylation of proteins, and TMT modification of peptide N-termini were set as variable modifications. The false discovery rate was set to less than 0.01, and peptide matches were filtered by a minimum peptide length of six amino acids. The reporter ion intensities of TMT-labeled peptides were used for the quantification of each protein. In the case of multiple unique peptides per protein identified, the average of the top three peptide areas were calculated.

Proteomic Data Analysis. The MS analysis data were analyzed using the TPP-R package as previously reported (Savitski et al., 2014). In TPP-TR experiments, the amount of each protein at 40°C was set to 1, and the amount of protein at each temperature point was calculated. The melting temperature (Tm) of each protein was determined as the temperature at which 50% of the protein is denatured. The following criteria were used to choose proteins altered their thermal stability: 1) The R^2 of the fitting curves for melting curves of vehicle and CNP-treated samples had to be >0.8; 2) the plateau of vehicle curve had to be <0.3; 3) the steepest slope of the protein melting curve had to be <-0.06; 4) the Tm difference between vehicle- and CNP-treated conditions was analyzed by Benjamini–Hochberg method, and the P value had to be <0.05 in one biologic replicates and <0.10 in the other; 5) the direction of thermal shift is the same in the two biologic replicates; 6) the difference of thermal shift between vehicle- and CNP-treated conditions was larger than the difference between lots of the vehicle. In TPP-CCR experiments, the vehicle condition was used as control for calculating fold-change. The fold-change values were transformed to a range between 0 and 1 for stabilized proteins, and 1 and 0 for destabilized proteins.

siRNA Knockdown. The siRNA molecules targeting GPX4 (GPX4 #1: SI00032536 and GPX2 #2: SI02627737) and a negative control siRNA (1022076) were purchased from Qiagen (Hilden, Germany). The siRNA molecules targeting ATG7 were purchased from Thermo Fisher Scientific (s20651). U-2 OS cells were transfected with the siRNAs using LipofectAMINE RNAiMAX Transfection Reagent (Thermo Fisher Scientific). Next day, the cells were plated onto 96-, 12-, or 6-well plates, incubated for 2 days, and then used for the AlphaLISA assay for p62 protein, lipid ROS detection, or Western blotting, respectively.

RNA Isolation and Quantitative Reverse Transcription Polymerase Chain Reaction. Total RNA was extracted from U-2 OS cells using the RNeasy Mini Kit (Qiagen). Total RNA was reverse-transcribed with ReverTra Ace qPCR RT Master Mix (Takara Bio), then the polymerase chain reaction was performed. We used the following specific primers and probes from Applied Biosystems (Foster City, CA): GPX4 (HS00989766_g1), ATG7 (Hs00893766_m1), p62 (HS01061917_g1) and glyceraldehyde-3-phosphate dehydrogenase (GAPDH) (4325792). The polymerase chain reaction was performed at 95°C for 10 minutes, and then 40 cycles of 95°C for 15 seconds, and 60°C for 1 minute using ABI Prism 7700 Sequence Detection System (Applied Biosystems).

AlphaLISA Assay for p62 Protein. Cells were lysed with AlphaLISA Lysis Buffer (PerkinElmer) containing EDTA-free protease inhibitor cocktail (Sigma-Aldrich) and incubated at room temperature for 10 minutes. The lysates were transferred to a white 1/2 AreaPlate-96 (PerkinElmer) and were incubated with AlphaLISA NaCl buffer containing 16.7 μg/ml anti-p62 antibody (M162-3) (MBL) conjugated acceptor beads and 0.42 nM biotinylated anti-p62 antibody (ab56416) (Abcam, Cambridge, UK) at room temperature for 1 hour. Then, streptavidin-coated donor beads (PerkinElmer) were added to each well at a final concentration of 40 μg/ml, and the plate was incubated for 30 minutes at room temperature. The p62 protein levels were measured using an EnVision-Alpha Reader (PerkinElmer). For measuring the total amount of protein, the cells were lysed using 0.1 N NaOH, and the protein concentration was determined by advanced protein assay reagent.

Western Blotting. Cells were lysed in radioimmunoprecipitation assay buffer [50 mM Tris-HCl buffer (pH 7.5), 150 mM NaCl, 1% NP-40, 0.5% sodium deoxycholate, 0.1% SDS, EDTA-free protease inhibitor cocktail, and phosphatase inhibitor cocktail (Nacalai Tesque, Inc., Kyoto, Japan)]. The cell lysates were centrifuged, and the supernatants were subjected to sodium dodecyl sulfate-polyacrylamide gel electrophoresis. After the electrophoresis, the proteins were transferred onto polyvinylidene fluoride membranes. The membranes were incubated with 5% skim milk for 1 hour at room temperature, the primary antibody overnight at 4°C, and then the secondary antibody for 1 hour at room temperature. The membranes were incubated with Immobilon Western Chemiluminescent HRP Substrate (Merck KGaA, Darmstadt, Germany), and the protein bands on the membranes were detected using a LAS3000 imager (Fujifilm, Tokyo, Japan). Densitometry analysis was done by Multi-Gauge software (Fujifilm).

Statistical Analysis. Data except for mass spectrometry analysis were analyzed by one-way ANOVA followed by Dunnett's test. P values less than 0.05 were considered significant. Based on the exploratory character of the study, the outcomes of the statistical tests should be interpreted as descriptive only.
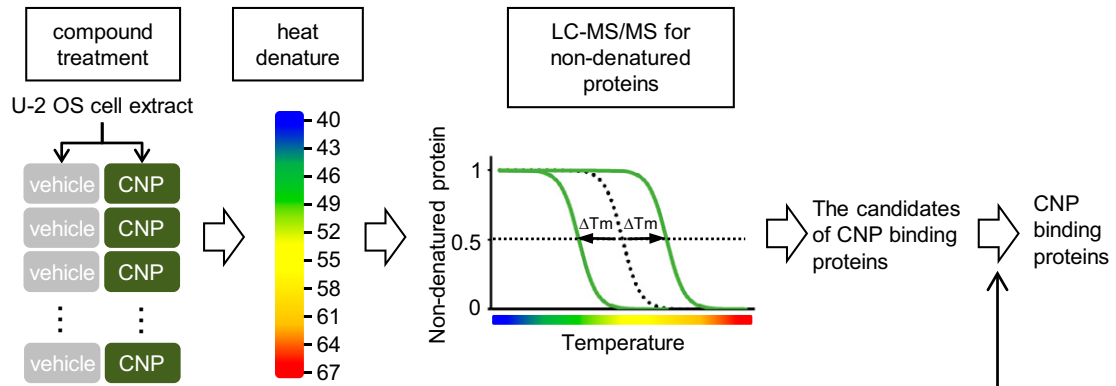
Results

CNP Induces Autophagy in an mTOR-Independent Manner. CNP is a vinca alkaloid extracted from the leaves of the tropical plant *T. divaricate* and possesses unique structure (Fig. 1A). It has been reported that CNP induces autophagy in HeLa cells or nerve growth factor-differentiated pheochromocytoma 12 cells (Sasazawa et al., 2015). Autophagy is a multistep process involved in the formation of the autophagosome, fusion of the autophagosome with the lysosome, and degradation of the contents in the autolysosome. The LC3 is a key biologic marker of autophagosome formation (Mizushima et al., 2010). Thus, we performed the LC3 puncta formation assay to assess the formation of autophagosomes in the CNP-treated human osteosarcoma cell line, U-2 OS. CNP treatment induced LC3 puncta formation in U-2

indicated proteins. Densitometric analysis was performed as described in *Materials and Methods*. The amounts of p-p70S6K or p-RPS6 were normalized to each total protein and were expressed as percent of vehicle control. Data are represented by box plots ($n = 3$ independent experiments). *$P < 0.05$ (one-way ANOVA with Dunnett's test) compared with vehicle control.
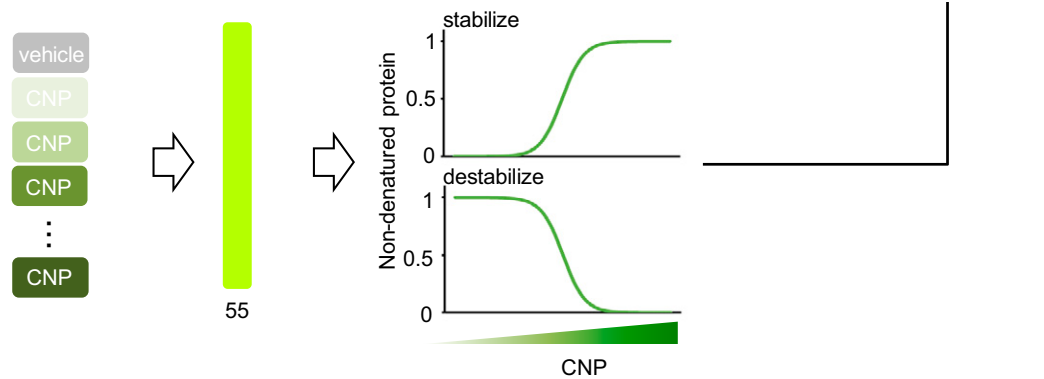
Fig. 2. Schematic workflow of the thermal proteome profiling procedure for identification of CNP-binding proteins. (A) TPP-TR experiments: U-2 OS cell extracts were incubated with vehicle or CNP and then divided into 10 aliquots, respectively. The aliquots were subjected to heating at the indicated temperatures, and centrifuged to remove denatured proteins. Nondenatured proteins were identified and quantified using LC-MS/MS, and melting curves were produced for each protein. The Tm of each protein was determined as the temperature at which 50% of the protein is denatured. The proteins with significantly altered Tm as a result of CNP treatment were selected as candidates for CNP-binding proteins. (B) TPP-CCR experiments: The candidates of CNP-binding proteins identified by TPP-TR experiments were validated by evaluating the CNP dose dependence of their thermal shifts. (C) The summary of TPP experiments. TPP-TR experiments were performed in biologic duplicates. The listed proteins were altered their Tm values with CNP treatment, and the alterations satisfied TPP-TR criteria as described in *Materials and Methods*. Accession name and gene name of the proteins were referred from UniProt Knowledgebase (https://www.uniprot.org/). In the column of TPP-CCR,
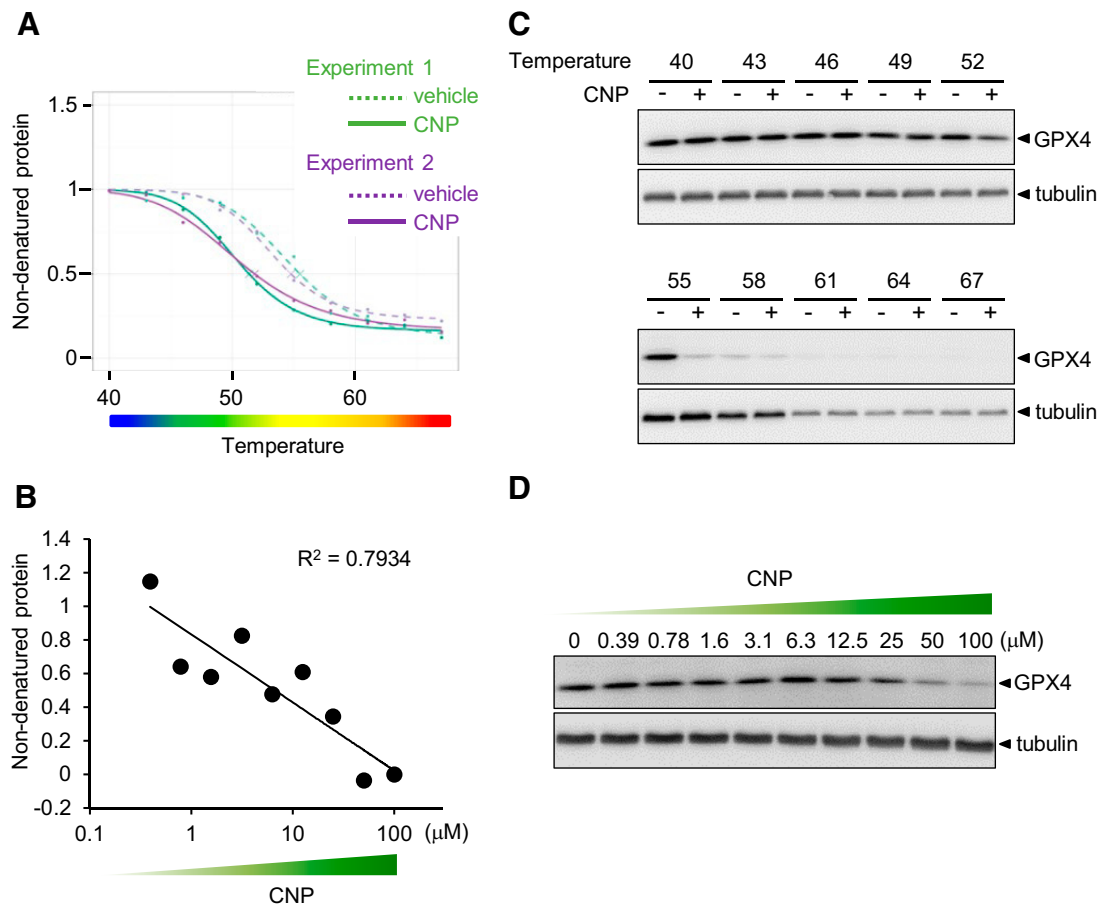
Fig. 3. CNP binds to GPX4 and reduces the thermal stability of GPX4 in a dose-dependent manner. (A) U-2 OS cell extracts were incubated for 10 minutes at 23°C with vehicle or 100 μM CNP, respectively. The extracts were subjected to heating at the indicated temperatures, and then centrifuged to remove denatured proteins. Nondenatured proteins were identified and quantified using LC-MS/MS as described in *Materials and Methods*. The melting curves for GPX4 in each condition were expressed as the ratio of vehicle-treated extracts heated at 40°C. The experiments were performed in biologic duplicates. (B) U-2 OS cell extracts were incubated with vehicle or CNP at nine different concentrations followed by heating at 55°C. Non-denatured proteins were identified and quantified using LC-MS/MS, and then the data were normalized and transformed as described in *Materials and Methods*. As a result of the data processing for GPX4, the fold-change value was one at the vehicle condition, and zero at the condition corresponding to the highest CNP concentration. (C and D) The samples were prepared as described above, and were analyzed by Western blotting using antibodies specific to the indicated proteins. α-tubulin was used as Western blotting internal control.

OS cells, and it further increased the number of puncta in the presence of the lysosome inhibitor bafilomycin A1 (Baf.A1). The results of CNP were similar to those of the autophagy inducer Torin 1 (Fig. 1B). Next, to confirm the degradation of the contents in the autolysosome, we measured the amount of p62/sequestosome-1 protein, which is an autophagy substrate. The experiment showed that the amount of p62 protein was decreased in CNP-treated U-2 OS cells, whereas the effects of CNP were eliminated in the presence of Baf.A1 (Fig. 1C). These results indicated that CNP induces autophagy in U-2 OS cells.

Furthermore, we examined whether the induction of autophagy was dependent on inhibition of the mammalian target of rapamycin (mTOR), also known as the mechanistic target of rapamycin. mTOR is a serine/threonine protein kinase, and functions as a negative regulator of autophagy. It is also known that Torin 1 induces autophagy by inhibiting

mTOR activity. Because CNP was previously shown to induce autophagy in an mTOR-independent manner, we investigated the effects of CNP on mTOR activity by measuring the phosphorylation of mTOR downstream effectors. CNP treatment had no effects on the phosphorylation of p70 S6 kinase (p70S6K) and S6 ribosomal protein (RPS6), whereas Torin 1 inhibited the phosphorylation of those proteins (Fig. 1, D and E). These results suggested that CNP induces autophagy in U-2 OS cells in an mTOR-independent manner. Therefore, the characteristic of the autophagy-inducing activity of CNP was identical with previous reports (Sasazawa et al., 2015).

Identification of CNP-Binding Proteins by TPP. TPP is based on the principle that proteins become thermally stabilized or destabilized when complexed with ligands. To elucidate the intracellular target protein of CNP, we used TPP to identify CNP-binding proteins as shown in Fig. 2.

the results were expressed as follows: Yes, the proteins were identified and quantified by mass spectrometry, and exhibited CNP-dose dependent thermal shifts; No, the proteins were identified and quantified by mass spectrometry, but not exhibited CNP-dose dependent thermal shifts; N.D., the proteins were not identified by mass spec analysis.
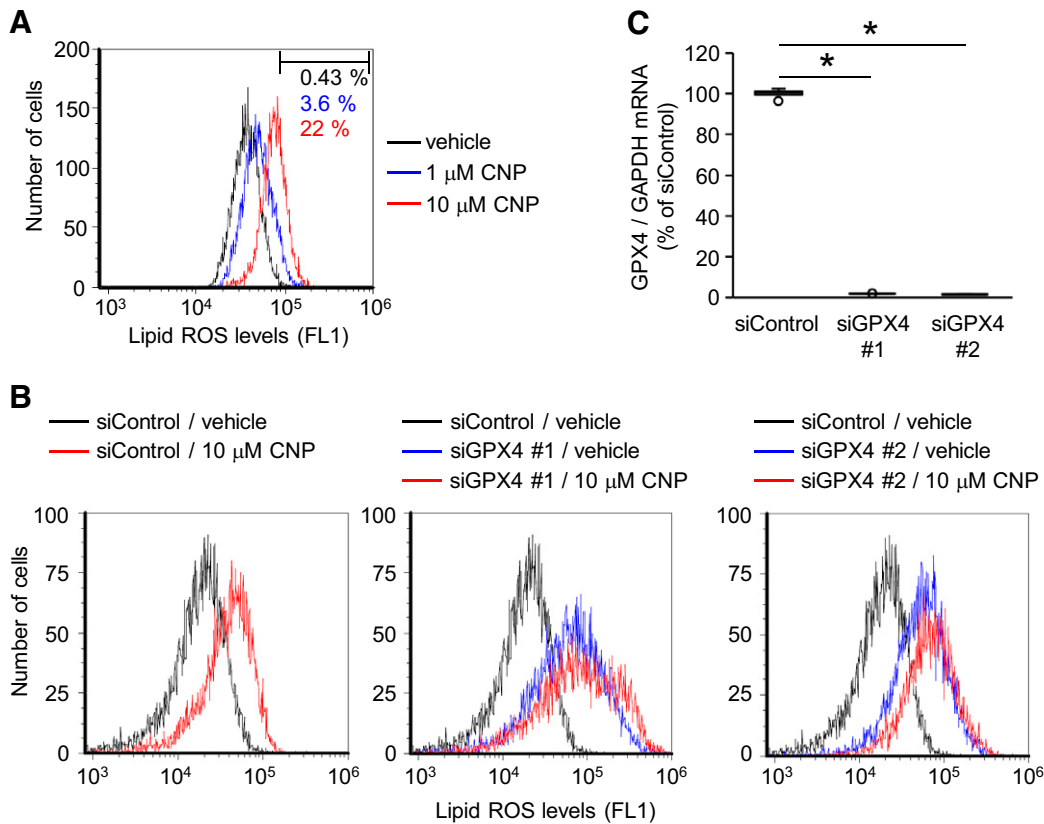
Fig. 4. CNP inhibits GPX4 activity and causes the accumulation of lipid ROS. (A) U-2 OS cells were incubated with CNP for 12 hours at the indicated concentration, and then incubated for 30 minutes with 10 mM boron-dipyrromethene 581/591 C11. Lipid ROS levels were assessed by flow cytometry. (B) U-2 OS cells were transfected with the indicated siRNAs at 10 nM. After incubation for 2 days, the cells were treated with CNP for 12 hours at the indicated concentration, and then assessed by flow cytometry to determine lipid ROS levels. (C) Two days after siRNA transfection, the cells were lysed and GPX4 mRNA levels were measured by quantitative reverse transcription polymerase chain reaction. The GPX4 mRNA levels were normalized to GAPDH mRNA levels, and were expressed as percent of control siRNA transfected cells. Data are represented by box plots ($n = 4$ technical replicates). The average Ct values of GAPDH were 19.8 (siControl), 20.2 (siGPX4 #1), and 19.7 (siGPX4 #2). *$P < 0.05$ (one-way ANOVA with Dunnett's test) compared with control siRNA transfected cells.

First, we performed TPP-TR experiments at a single CNP concentration. The compound concentration required for the changing thermal stability tends to be about 10 times higher than that of affinity for compound-binding proteins (Savitski et al., 2014). For this reason, we adopted the concentration of CNP at 100 μM in TPP-TR experiments to avoid missing the CNP-binding proteins. The cell extracts were heated to 40–67°C in the presence of 100 μM CNP or DMSO as a vehicle control. Then, nondenatured proteins were quantified using mass spectrometry (MS). In the course of TPP-TR experiments, through assessing the effect of CNP treatment on the thermal stability of approximately 8000 proteins, 17 proteins were identified as candidates of CNP-binding proteins (Fig. 2C; Supplemental Table 1). Their Tm values in TPP-TR experiments were altered with CNP treatment, and the alterations satisfied TPP-TR criteria as described in a previous report (Savitski et al., 2014). In the experiments, the thermal stability of GPX4 was destabilized by CNP treatment (Fig. 2C and 3A). In the process of selecting the candidates, we fitted the relative protein abundances at each temperature by sigmoidal curves, and then calculated Tm values. Thus, curve fitting and determining of Tm values play crucial roles in TPP-TR experiments. However, the shape of the sigmoidal curve is easily affected by the

technical and/or the biologic variation in quantitative proteomics. Especially, proteomic analysis for low abundance proteins is challenging. In addition, it is known that protein structure intermediates are often present in the process of transitioning from the folded state to the denatured state (El-Baba et al., 2017). These proteins exhibited complex sigmoidal curves, which are not ideal. For these reasons, the strategy using curve fitting and extraction of Tm values from the curves has the potential to provide false positives as TPP-TR artifacts. To validate the alteration of their thermal stability, we performed TPP-CCR experiments to evaluate the CNP dose dependence for the thermal shifts of the candidate proteins. As a result, we had evaluated 5 proteins out of 17 proteins that were identified by TPP-TR experiments, and only GPX4 exhibited dose-dependent thermal shift (Figs. 2C and 3B; Supplemental Table 2). Thus, we concluded that 4 proteins except for GPX4 were TPP-TR artifacts. Although the possibility remains that the other 12 proteins were CNP-binding proteins, we further validated the results of MS analysis for GPX4. We performed Western blotting analysis of GPX4 using samples prepared in the same manner for MS analysis. The results of these experiments as well as MS analysis showed that GPX4 was thermally destabilized by CNP treatment (Fig. 3, C and D). Furthermore, GPX1 or
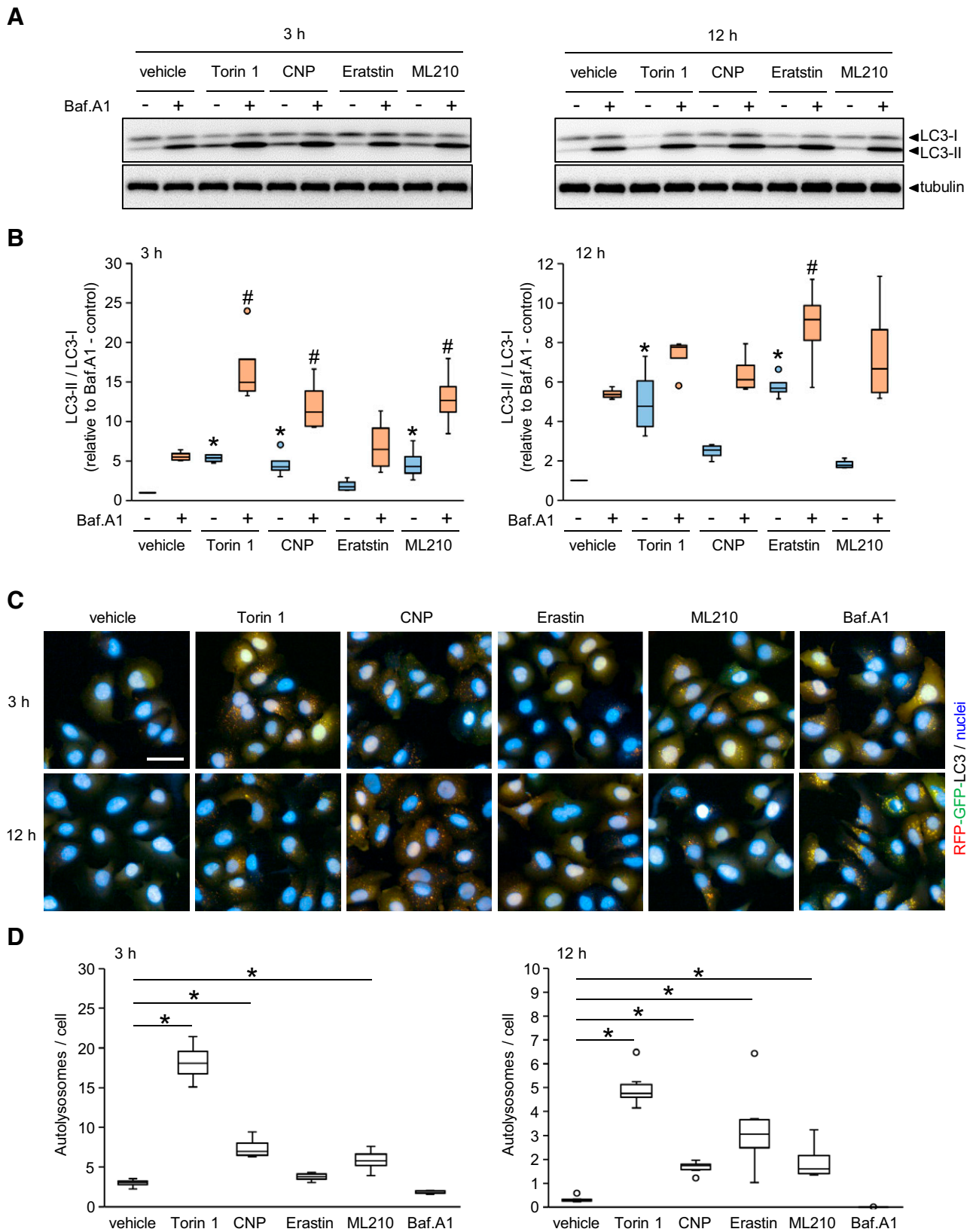
A

B

C

D

Fig. 5. Similar with CNP treatment, GPX4 inhibitor induces autophagy. (A and B) U-2 OS cells were incubated for 3 or 12 hours in the presence of the indicated compounds. The cells were lysed and analyzed by Western blotting using antibodies specific to the indicated proteins. The ratio of LC3-II/LC3-I was evaluated by densitometry analysis. Data are represented by box plots ($n = 4$ independent experiments). *$P < 0.05$ (one-way ANOVA with Dunnett's test) compared with Baf.A1-untreated vehicle control, #$P < 0.05$ (one-way ANOVA with Dunnett's test) compared with Baf.A1-treated vehicle control. (C and D) U-2 OS cells stably expressing RFP-GFP-LC3 were incubated for 3 or 12 hours with the indicated compounds. The cells were fixed with 4% formaldehyde and stained for nuclei (blue) as described in *Materials and Methods*. The cells were observed

GPX7, belonging to the GPX family, did not have altered thermal stability with CNP treatment (Supplemental Fig. 1). These results suggested that GPX4 is a CNP-binding protein.

CNP Inhibits GPX4 Activity and Causes the Accumulation of Lipid ROS in U-2 OS Cells. It is known that GPX4 is an antioxidant peroxidase that directly reduces phospholipid hydroperoxide, and that inhibition of GPX4 results in accumulation of lipid ROS in cells (Brigelius-Flohé and Maiorino, 2013). In addition, it has been reported that some GPX4 inhibitors induce autophagy as confirmed by LC3 puncta formation and the conversion of LC3-I to LC3-II form (Hou et al., 2016; Wang et al., 2019). As previously reported, the amount of LC3 puncta and LC3-II form correlates with the quantity of autophagosomes (Mizushima et al., 2010). Therefore, we hypothesized that CNP inhibits the hydrolase activity of GPX4, resulting in accumulation of lipid ROS in cells, which may lead to the induction of autophagy. To evaluate the effects of CNP on GPX4 activity, we measured the amount of lipid ROS in cells incubated with or without CNP. As expected, when we treated U-2 OS cells with CNP for 12 hours, the amount of lipid ROS was increased in a dose-dependent manner (Fig. 4A). In addition, we carried out GPX4 knockdown experiments to confirm whether the increase of lipid ROS was indeed due to the inhibition of GPX4 activity. CNP treatment induced accumulation of lipid ROS in control siRNA transfected cells, whereas the effect of CNP was abolished in GPX4-knockdown cells (Fig. 4B). In the knockdown experiments, GPX4 mRNA was decreased by GPX4 siRNA transfection (Fig. 4C). Thus, we consider that lipid ROS accumulation in CNP-treated cells was dependent on GPX4 inhibition. These results suggested that CNP inhibits GPX4 activity, and thereby leads to the accumulation of lipid ROS in cells.

GPX4 Inhibition Induces Autophagy in U-2 OS Cells. To evaluate the effects of GPX4 inhibition on induction of autophagy, we investigated whether the GPX4 inhibitors, ML210 and erastin, can induce autophagy in cells. ML210 is an alkylating agent that covalently binds to the selenocysteine residue, which is a component of the GPX4 active site, and directly suppresses GPX4 enzymatic activity (Eaton et al., 2020). On the other hand, erastin inhibits cystine uptake by the cystine/glutamate antiporter (system x_c^-), and then decreases intracellular glutathione levels in cells. This consequently suppresses GPX4 activity indirectly (Dixon et al., 2012).

First, we assessed the conversion of LC3-I to LC3-II form in cells treated with GPX4 inhibitors. When we treated U-2 OS cells for 3 hours with ML210, the amount of LC3-II form was increased, and this was further increased with Baf.A1 cotreatment (Fig. 5, A and B). The results were similar to those of the autophagy inducer Torin 1 or CNP. On the other hand, considering erastin treatment, we detected LC3-II conversion 12 hours after the treatment, which was later than that detected in ML210-treated cells (Fig. 5, A and B). This seemed to reflect erastin's pharmacological action as an indirect GPX4 inhibitor.

Next, the LC3 puncta formation assay was performed in U-2 OS cells stably expressing RFP-GFP-LC3. In a low-pH environment, RFP fluorescence is stable, whereas GFP fluorescence will be quenched. Yellow fluorescence, representing colocalization of RFP and GFP, indicates autophagosomes not fused with acidic lysosomes. Therefore, red punctate fluorescence will increase if autophagy is enhanced, whereas only yellow punctate fluorescence will be evident if autophagy is inhibited. The experiment showed that the number of autolysosomes, which is RFP positive and GFP negative, was increased in ML210-, erastin-, and CNP-treated cells. The results were comparable to that of Torin 1 treatment. Conversely, the number of LC3 yellow puncta was increased in the lysosome inhibitor Baf.A1 (Fig. 5, C and D).

Finally, we investigated the effects of GPX4 knockdown on the expression of p62 protein levels. As expected, the p62 protein levels were downregulated in GPX4-knockdown cells (Fig. 6A). To confirm the downregulation of p62 protein levels were the result of autophagy activation, we assessed p62 mRNA levels in GPX4-knockdown cells. The experiment showed that GPX4 knockdown had no effects on p62 mRNA levels (Fig. 6B). These results indicated that the effect of CNP on the downregulation of p62 protein levels seemed to reflect autophagy induction, but not inhibition of its mRNA expression. Simultaneously, we performed ATG7 knockdown, which is an essential autophagy protein, as an experimental control. As a result of ATG7 knockdown, p62 protein and p62 mRNA levels were upregulated (Fig. 6, A and B). The upregulation of p62 protein levels seemed to reflect autophagy inhibition and the induction of p62 mRNA expression. Furthermore, we assessed the phosphorylation of mTOR downstream effectors p70S6K and RPS6 in GPX4-knockdown cells. The experiments showed that the phosphorylation of those remained unchanged (Fig. 6, C and D). These results strongly suggested that GPX4 inhibition leads to autophagy activation, and that CNP treatment and GPX4 knockdown produce similar phenotypes.

Discussion

There are eight isoforms of GPXs in humans, with differences in their tissue expression and substrate specificity (Brigelius-Flohé and Maiorino, 2013). GPXs catalyze the reduction of hydrogen peroxide and organic hydroperoxides to water or corresponding alcohols, thereby acting as antioxidants. Recently, it has also become clear that GPX4 is involved in cell death called ferroptosis, which is different from necrosis and apoptosis. Among GPX family members, only GPX4 inhibition induces cell death and thus is a key regulator of ferroptosis (Yang et al., 2014). It has been reported that ferroptosis may be a type of autophagic cell death, and although autophagy maintains homeostasis, excessive autophagy induces autophagy-dependent cell death (Gao et al., 2016; Su et al., 2019). In fact, various types of GPX4 inhibitors induce autophagy and ferroptosis (Hou et al., 2016; Wang et al., 2019). In this study, we found that CNP, one type of autophagy inducer, inhibits GPX4 activity.
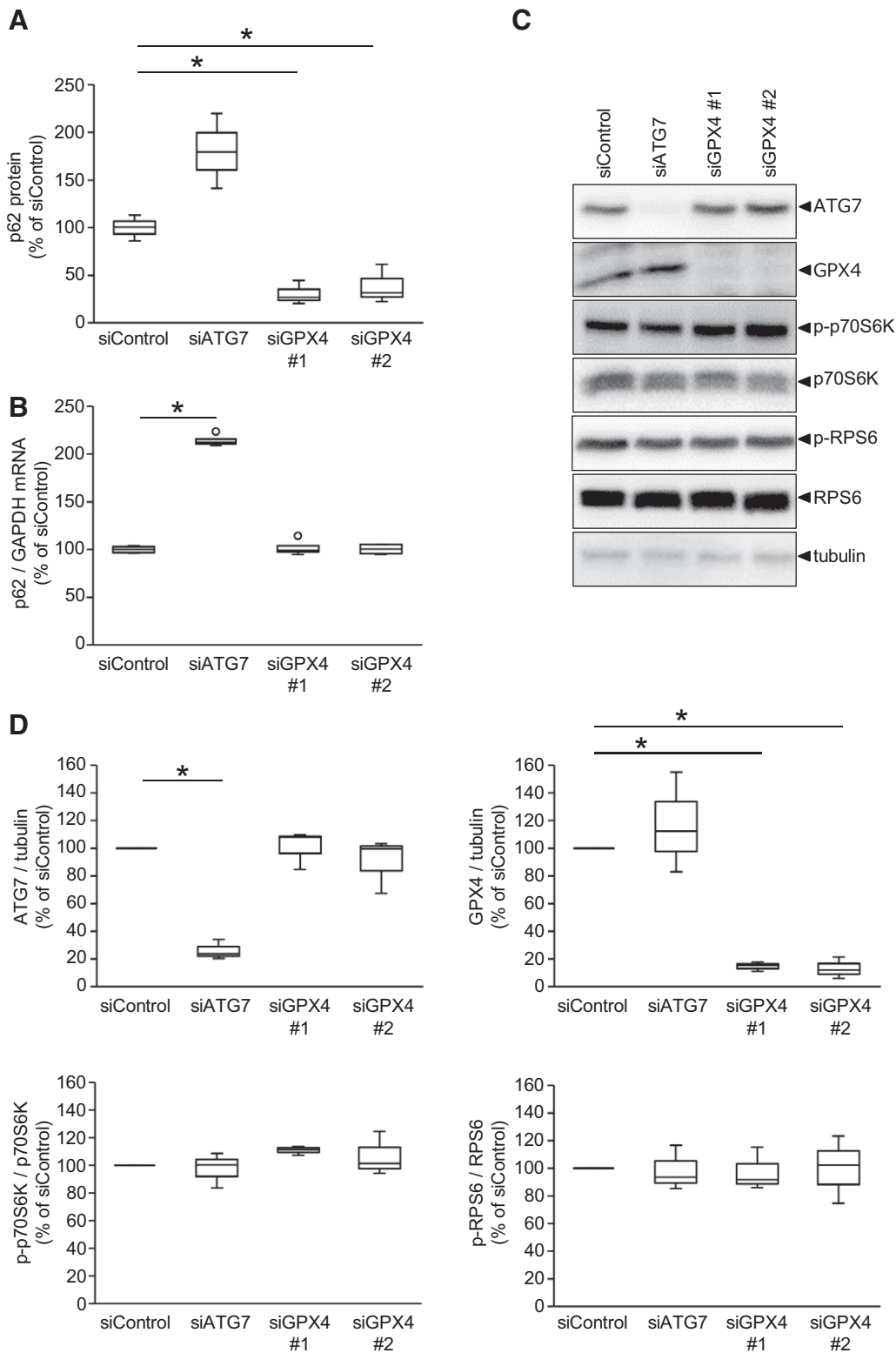
by using the Operetta CLS system. Scale bar, 50 μm. The number of autolysosomes (dot of LC3 with RFP positive and GFP negative) per cell were counted using Operetta CLS. Data are represented by box plots ($n = 6$ biologic replicates). *$P < 0.05$ (one-way ANOVA with Dunnett's test) compared with vehicle control.

Fig. 6. Similar with CNP treatment, knockdown of GPX4 induces autophagy. (A) U-2 OS cells were transfected with the indicated siRNAs at 10 nM and incubated for 3 days. The cells were lysed, and p62 protein levels were measured by AlphaLISA. The p62 protein levels were normalized to the total protein levels, and were expressed as percent of control siRNA transfected cells. Data are represented by box plots ($n = 3$ biologic replicates). (B) The siRNAs transfected cells were lysed, and mRNA levels were measured by quantitative reverse transcription polymerase chain reaction. The p62 and ATG7 mRNA levels were normalized to GAPDH mRNA levels, and were expressed as percent of control siRNA transfected cells. Data are represented by box plots ($n = 4$ technical replicates). The average Ct values of GAPDH were 18.7 (siControl), 19.2 (siATG7), 18.9 (siGPX4 #1), and 18.9 (siGPX4 #2). (C and D) The siRNA transfected cells were lysed and analyzed by Western blotting using antibodies specific to the indicated proteins. The amounts of ATG7 and GPX4 were normalized to α-tubulin, and were expressed as percent of control siRNA transfected cells. Densitometric analysis was performed as described in *Materials and Methods*. The amounts of p-p70S6K or p-RPS6 were normalized to each total protein and were expressed as percent of control siRNA transfected cells. Data are represented by box plots ($n = 3$ independent experiments). *$P < 0.05$ (one-way ANOVA with Dunnett's test) compared with control siRNA transfected cells.

First, our experiments indicated that GPX4 is a direct binding protein of CNP (Fig. 3). Although we did not evaluate whether CNP can directly inhibit the hydrolase activity of GPX4 in vitro, we showed the accumulation of lipid ROS in CNP-treated cells (Fig. 4A). In contrast to other GPX isoforms, the active site of GPX4 does not contain an exposed surface loop (Scheerer et al., 2007). With this unique structure, GPX4 can catalyze phospholipids or cholesterol hydroperoxides incorporated in membranes or lipoproteins. Thus, it is generally believed that the increasing amount of lipid ROS indicates the inhibition of GPX4 hydrolase activity in cells. In fact, GPX4 knockdown induced accumulation of lipid ROS in cells (Fig. 4B). In addition, although U-2 OS cells express three GPX isoforms (GPX1, GPX4, and GPX7) as determined by MS analysis, only the thermal stability of GPX4 had changed with CNP treatment (Fig. 3A; Supplemental Fig. 1). These results support the hypothesis that CNP specifically suppresses the hydrolase activity of GPX4 in cells.

Next, we showed that two known GPX4 inhibitors increase the amount of LC3-II form and the number of autolysosomes (Fig. 5). Furthermore, we found that, as with CNP treatment, GPX4 deficiency decreases p62 protein levels, but not at mRNA levels (Fig. 6, A and B). These results strongly support the hypothesis that GPX4 inhibition induces autophagy. Unfortunately, the precise mechanism by which accumulation of lipid ROS by GPX4 inhibition promotes autophagy is unknown. Meanwhile, we showed CNP treatment or GPX4 knockdown had no effects on enzyme activity of mTOR, which is a well known pathway for autophagy regulation (Figs. 1, C and D and 6, C and D). The results indicated that lipid ROS accumulation affects the signaling pathway leading to autophagy in an mTOR-independent manner. One possibility is that oxidized lipids activate autophagy by inhibiting the c-Jun N-terminal kinase (JNK) signaling pathway. It has been reported that the lipid peroxidation product, 4-hydroxynonenal or malondialdehyde, activates JNK (Haberzettl and Hill, 2013). JNK activation can dissociate the interaction between Beclin-1 and B-cell lymphoma 2 by phosphorylating B-cell lymphoma 2. It leads to activation of vacuolar protein sorting 34, one of the key kinases involved in autophagy, and then to induction of mTOR-independent activation of autophagy (Wei et al., 2015). Further analysis is required to uncover the precise mechanisms of autophagy induction by inhibiting GPX4.

In a previous report, ADP-ribosylation factor-like protein 6-interacting protein 1 (ARL6ip1) was identified as a CNP-binding protein using CNP-immobilized beads (Suzuki et al., 2009). Also, they determined its essential binding region for CNP (Kuroda et al., 2013). ARL6ip1 is localized at the endoplasmic reticulum membrane and negatively regulates apoptosis (Lui et al., 2003). However, in ARL6ip1-knockdown cells, CNP induced the conversion of LC3-I to LC3-II form as well as control cells (Sasazawa et al., 2015). Therefore, it is assumed that CNP induces autophagy independently of ARL6ip1. Affinity purification using compound-immobilized beads is one of the most prevalent methods for target identification of bioactive compounds (Saxena et al., 2009; Kawatani and Osada, 2014). However, modifying the compounds in preparation for immobilization on beads sometimes decreases the affinity of the compound to the target protein. Furthermore, it is possible that the interaction of the compound and

the target protein may be prevented by steric hindrance of the beads. For these reasons, development of techniques to identify compound-binding proteins without chemical modification has been expected. In this study, we investigated the underlying mechanism of CNP's action in autophagy induction using the TPP technique. The technique applied the Cellular Thermal Shift Assay to proteomics analysis, and can be used for identifying the target proteins of compounds without chemical modification (Martinez-Molina et al., 2013). As expected, in this study, GPX4 could be identified as a new CNP-binding protein. Therefore, this technique was shown to be a powerful tool for identifying binding proteins of bioactive molecules, especially natural compounds that have structures difficult-to-modify.

Since GPX4 is a suppressor protein of ferroptosis, we investigated whether CNP treatment induces ferroptosis. As previously reported, overnight treatment of CNP decreased U-2 OS cell numbers. However, the decreasing was not suppressed by ferroptosis inhibitors, ferrostatin-1 (data not shown). CNP is a natural compound, so that it is possible to bind a lot of proteins. In fact, CNP might be inhibited apoptosis repressor ARL6ip1, which is one of the CNP-binding proteins, and then induced apoptosis. Therefore, it could be difficult to detect the effect of CNP treatment on ferroptosis. Further analysis is required to clarify the relationship between CNP and ferroptosis.

From the findings of this work, we concluded that TPP is a useful technique for analyzing the mechanism of natural compounds. Using this technique, we identified GPX4 as a new binding protein of CNP, and showed that the autophagy promoting activity of CNP is mediated by GPX4 inhibition.

Authorship Contributions

Participated in research design: Kakegawa, Hosoi, Ozawa, Hatanaka.

Conducted experiments: Kakegawa, Ohtsuka, Yokoyama.

Performed data analysis: Kakegawa, Ohtsuka.

Wrote or contributed to the writing of the manuscript: Kakegawa, Hosoi, Ozawa.

References

Brigelius-Flohé R and Maiorino M (2013) Glutathione peroxidases. *Biochim Biophys Acta* **1830**:3289–3303.

Dixon SJ, Lemberg KM, Lamprecht MR, Skouta R, Zaitsev EM, Gleason CE, Patel DN, Bauer AJ, Cantley AM, Yang WS, et al. (2012) Ferroptosis: an iron-dependent form of nonapoptotic cell death. *Cell* **149**:1060–1072.

Eaton JK, Furst L, Ruberto RA, Moosmayer D, Hilpmann A, Ryan MJ, Zimmermann K, Cai LL, Niehues M, Badock V, et al. (2020) Selective covalent targeting of GPX4 using masked nitrile-oxide electrophiles. *Nat Chem Biol* **16**:497–506.

El-Baba TJ, Woodall DW, Raab SA, Fuller DR, Laganowsky A, Russell DH, and Clemmer DE (2017) Melting proteins: Evidence for multiple stable structures upon thermal denaturation of native ubiquitin from ion mobility spectrometry-mass spectrometry measurements. *J Am Chem Soc* **139**:6306–6309.

Feher M and Schmidt JM (2003) Property distributions: differences between drugs, natural products, and molecules from combinatorial chemistry. *J Chem Inf Comput Sci* **43**:218–227.

Galluzzi L, Baehrecke EH, Ballabio A, Boya P, Bravo-San Pedro JM, Cecconi F, Choi AM, Chu CT, Codogno P, Colombo MI, et al. (2017) Molecular definitions of autophagy and related processes. *EMBO J* **36**:1811–1836.

Gao M, Monian P, Pan Q, Zhang W, Xiang J, and Jiang X (2016) Ferroptosis is an autophagic cell death process. *Cell Res* **26**:1021–1032.

Haberzettl P and Hill BG (2013) Oxidized lipids activate autophagy in a JNK-dependent manner by stimulating the endoplasmic reticulum stress response. *Redox Biol* **1**:56–64.

Harvey AL, Edrada-Ebel R, and Quinn RJ (2015) The re-emergence of natural products for drug discovery in the genomics era. *Nat Rev Drug Discov* **14**:111–129.

Hou W, Xie Y, Song X, Sun X, Lotze MT, Zeh 3rd HJ, Kang R, and Tang D (2016) Autophagy promotes ferroptosis by degradation of ferritin. *Autophagy* **12**:1425–1428.

Kam TS, Loh KY, and Wei C (1993) Conophylline and conophyllidine: new dimeric alkaloids from *Tabernaemontana divaricata*. *J Nat Prod* **56**:1865–1871.

Kawatani M and Osada H (2014) Affinity-based target identification for bioactive small molecules. *MedChemComm* **5**:277–287.

Kuroda M, Funasaki S, Saitoh T, Sasazawa Y, Nishiyama S, Umezawa K, and Simizu S (2013) Determination of topological structure of ARL6ip1 in cells: identification of the essential binding region of ARL6ip1 for conophylline. *FEBS Lett* **587**: 3656–3660.

Lachance H, Wetzel S, Kumar K, and Waldmann H (2012) Charting, navigating, and populating natural product chemical space for drug discovery. *J Med Chem* **55**:5989–6001.

Lui HM, Chen J, Wang L, and Naumovski L (2003) ARMER, apoptotic regulator in the membrane of the endoplasmic reticulum, a novel inhibitor of apoptosis. *Mol Cancer Res* **1**:508–518.

Mahul-Mellier AL, Fauvet B, Gysbers A, Dikiy I, Oueslati A, Georgeon S, Lamontanara AJ, Bisquerrt A, Eliezer D, Masliah E, et al. (2014) c-Abl phosphorylates α-synuclein and regulates its degradation: implication for α-synuclein clearance and contribution to the pathogenesis of Parkinson's disease. *Hum Mol Genet* **23**:2858–2879.

Mizushima N (2018) A brief history of autophagy from cell biology to physiology and disease. *Nat Cell Biol* **20**:521–527.

Mizushima N, Yoshimori T, and Levine B (2010) Methods in mammalian autophagy research. *Cell* **140**:313–326.

Mizushima N and Levine B (2020) Autophagy in human diseases. *N Engl J Med* **383**:1564–1576.

Martinez-Molina D, Jafari R, Ignatushchenko M, Seki T, Larsson EA, Dan C, Sreekumar L, Cao Y, and Nordlund P (2013) Monitoring drug target engagement in cells and tissues using the cellular thermal shift assay. *Science* **341**:84–87.

Nakamura S, Oba M, Suzuki M, Takahashi A, Yamamuro T, Fujiwara M, Ikenaka K, Minami S, Tabata N, Yamamoto K, et al. (2019) Suppression of autophagic activity by Rubicon is a signature of aging. *Nat Commun* **10**:847.

Newman DJ and Cragg GM (2016) Natural products as sources of new drugs from 1981 to 2014. *J Nat Prod* **79**:629–661.

Ogata T, Li L, Yamada S, Yamamoto Y, Tanaka Y, Takei I, Umezawa K, and Kojima I (2004) Promotion of beta-cell differentiation by conophylline in fetal and neonatal rat pancreas. *Diabetes* **53**:2596–2602.

Ohashi T, Nakade Y, Ibusuki M, Kitano R, Yamauchi T, Kimoto S, Inoue T, Kobayashi Y, Sumida Y, Ito K, et al. (2019) Conophylline inhibits high fat diet-induced non-alcoholic fatty liver disease in mice. *PLoS One* **14**:e0210068.

Ohsumi Y (2001) Molecular dissection of autophagy: two ubiquitin-like systems. *Nat Rev Mol Cell Biol* **2**:211–216.

Rosén J, Gottfries J, Muresan S, Backlund A, and Oprea TI (2009) Novel chemical space exploration via natural products. *J Med Chem* **52**:1953–1962.

Saito R, Yamada S, Yamamoto Y, Kodera T, Hara A, Tanaka Y, Kimura F, Takei I, Umezawa K, and Kojima I (2012) Conophylline suppresses pancreatic stellate cells and improves islet fibrosis in Goto-Kakizaki rats. *Endocrinology* **153**:621–630.

Sasazawa Y, Sato N, Umezawa K, and Simizu S (2015) Conophylline protects cells in cellular models of neurodegenerative diseases by inducing mammalian target of rapamycin (mTOR)-independent autophagy. *J Biol Chem* **290**:6168–6178.

Savitski MM, Reinhard FB, Franken H, Werner T, Savitski MF, Eberhard D, Martinez Molina D, Jafari R, Dovega RB, Klaeger S, et al. (2014) Tracking cancer drugs in living cells by thermal profiling of the proteome. *Science* **346**:1255784.

Saxena C, Higgs RE, Zhen E, and Hale JE (2009) Small-molecule affinity chromatography coupled mass spectrometry for drug target deconvolution. *Expert Opin Drug Discov* **4**:701–714.

Scheerer P, Borchert A, Krauss N, Wessner H, Gerth C, Höhne W, and Kuhn H (2007) Structural basis for catalytic activity and enzyme polymerization of phospholipid hydroperoxide glutathione peroxidase-4 (GPx4). *Biochemistry* **46**:9041–9049.

Su LJ, Zhang JH, Gomez H, Murugan R, Hong X, Xu D, Jiang F, and Peng ZY (2019) Reactive oxygen species-induced lipid peroxidation in apoptosis, autophagy, and ferroptosis. *Oxid Med Cell Longev* **2019**:5080843.

Suzuki E, Ogura H, Kato K, Takei I, Kabe Y, Handa H, and Umezawa K (2009) Preparation of conophylline affinity nano-beads and identification of a target protein. *Bioorg Med Chem* **17**:6188–6195.

Tezuka T, Ota A, Karnan S, Matsuura K, Yokoo K, Hosokawa Y, Vigetti D, Passi A, Hatano S, Umezawa K, et al. (2018) The plant alkaloid conophylline inhibits matrix formation of fibroblasts. *J Biol Chem* **293**:20214–20226.

Umezawa K, Hiroki A, Kawakami M, Naka H, Takei I, Ogata T, Kojima I, Koyano T, Kowithayakorn T, Pang HS, et al. (2003) Induction of insulin production in rat pancreatic acinar carcinoma cells by conophylline. *Biomed Pharmacother* **57**:341–350.

Umezawa K, Ohse T, Yamamoto T, Koyano T, and Takahashi Y (1994) Isolation of a new vinca alkaloid from the leaves of Ervatamia microphylla as an inhibitor of ras functions. *Anticancer Res* **14** (6B):2413–2417.

Wang X, Lu S, He C, Wang C, Wang L, Piao M, Chi G, Luo Y, and Ge P (2019) RSL3 induced autophagic death in glioma cells via causing glycolysis dysfunction. *Biochem Biophys Res Commun* **518**:590–597.

Wei Y, An Z, Zou Z, Sumpter Jr R, Su M, Zang X, Sinha S, Gaestel M, and Levine B (2015) The stress-responsive kinases MAPKAPK2/MAPKAPK3 activate starvation-induced autophagy through Beclin 1 phosphorylation. *eLife* **4**:e05289.

Yang WS, SriRamaratnam R, Welsch ME, Shimada K, Skouta R, Viswanathan VS, Cheah JH, Clemons PA, Shamji AF, Clish CB, et al. (2014) Regulation of ferroptotic cancer cell death by GPX4. *Cell* **156**:317–331.

Address correspondence to: Junya Kakegawa, Pharmaceutical Frontier Research Laboratories, Central Pharmaceutical Research Institute, Japan Tobacco Inc., 1-13-2, Fukuura, Kanazawa-Ku, Yokohama, Kanagawa 236-0004, Japan. E-mail: junya.kakegawa@jt.com